A Chemical Solution Approach to Epitaxial Metal Nitride Thin Films

By *Hongmei Luo,* Yuan Lin, Haiyan Wang, Joon Hwan Lee, Natalya A. Suvorova, Alexander H. Mueller, Anthony K. Burrell, T. Mark McCleskey, Eve Bauer, Igor O. Usov, Marilyn E. Hawley, Terry G. Holesinger,* and *Quanxi Jia**

Nitride thin films are used in many applications due to their strong hardness, chemical resistance, and unique electronic properties. In particular, their applications in electronic and optoelectronic devices have recently spurred considerable interest. For example, GaN and AlN have been extensively investigated for lighting applications.[1] Furthermore, it is well known that TiN is highly conductive, while AlN is highly resistive and transparent.[2,3] The solid-solution of $Ti_{1-x}Al_xN$ can potentially have properties of both the TiN and the AlN. Several techniques have been used to grow nitride films, including magnetron sputtering,[4–13] ion-beam sputtering,[14] ion-beam-assisted deposition,[15] arc evaporation,[16] molecular- beam epitaxy,[17–19] pulsed-laser deposition,[20–23] atomic-layer deposition,[2] halide-vapor transport epitaxy,[24] and metalorganic,[3,25] plasma-enhanced,[26–28] or atmospheric-pressure chemical-vapor deposition (CVD).[29–31] Even with the abundance of synthetic routes to nitride films, challenges still remain in obtaining high-quality epitaxial nitride films. In general, the difficulty in the heteroepitaxial growth of such films lies in the large mismatches in either lattice parameters or thermal- expansion coefficients between the film and the substrate.[32] Nitride films with rough surface morphologies and high densities of defects are often observed.[32]

[*] Dr. H. M. Luo, Dr. A. K. Burrell, Dr. T. M. McCleskey, E. Bauer
Dr. T. G. Holesinger, Dr. Q. X. Jia
Materials Physics and Applications Division
Los Alamos National Laboratory
Los Alamos, NM 87545 (USA)
E-mail: hluo@lanl.gov; qxjia@lanl.gov
Dr. Y. Lin
School of Microelectronics and Solid State Electronics
University of Electronic Science and Technology of China
Chengdu 610054 (P.R. China)
Dr. H. Wang, J. H. Lee
Department of Electrical and Computer Engineering
Texas A&M University
College Station, TX 77843 (USA)
Dr. N. A. Suvorova, Dr. I. O. Usov, Dr. M. E. Hawley
Materials Science and Technology Division
Los Alamos National Laboratory
Los Alamos, NM 87545 (USA)
Dr. A. H. Mueller
Chemistry Division, Los Alamos National Laboratory
Los Alamos, NM 87545 (USA)

DOI: 10.1002/adma.200801959

All of the above-reported deposition routes[2–28] to epitaxial nitride films have the common feature of requiring vacuum systems. An alternative approach for the fabrication of thin films is the chemical solution deposition method, where a precursor solution is deposited by spin- or dip-coating onto a single-crystal substrate.[33] This technique offers advantages in terms of cost, setup, and the ability to coat large areas. Chemical solution deposition of metal nitride films is very useful in semiconductor technology. However, there are very limited reports on the growth of nitride films (GaN only) using this technique.[34–40] The precursors used in earlier investigations on GaN are not widely available and are difficult to handle due to their sensitivity to air. In addition, the morphology of the GaN films needs further improvement, as the films were very often non-continuous, leading to porous or cracked surfaces.[34–38] To date, no other metal nitride films were reported by chemical solution deposition. It is apparent that a general chemical solution approach to prepare metal nitride thin films should be developed. In this communication, we report the growth of epitaxial cubic TiN, metastable cubic AlN, and solid-solution $Ti_{1-x}Al_xN$ films with smooth surface morphologies from polymer-assisted deposition (PAD). In the PAD process, metal–polymer solutions were used as film precursors, where commercially available water-soluble polymers were used. The polymers not only control the solution viscosity but also bind the metal ions to form a homogenous distribution of ions in the solutions.[41,42]

The procedures to forming nitride films comprise the following two steps: i) formation of homogenous metal polymeric liquid precursors by binding the polymer with metal ions; ii) thermolysis and ammonolysis of the coated films in flowing ammonia gas to yield the metal nitride films. The mechanism of formation of metal nitrides through a solution approach has been discussed.[34–40] The main advantage of the PAD approach is that many metal ions can bind to polyethyleneimine (PEI) and/or ethylenediaminetetraacetic acid (EDTA) to form very stable precursor solutions, which are stable in air and water for months.[42] Notably, this is the first report of chemical solution approach to TiN, AlN, and mixed nitride films.

The X-ray diffraction (XRD) patterns for TiN, AlN, and mixed $Ti_{1-x}Al_xN$ films on $SrTiO_3$ (STO) substrates are similar, since the lattice parameters of cubic TiN and AlN are very close ($a = 0.41$ nm), with a lattice mismatch of around 5% with STO ($a = 0.3905$ nm). Figure 1a and b show the XRD results from the θ–2θ scan and ϕ-scans of TiN on STO annealed at 900 °C.

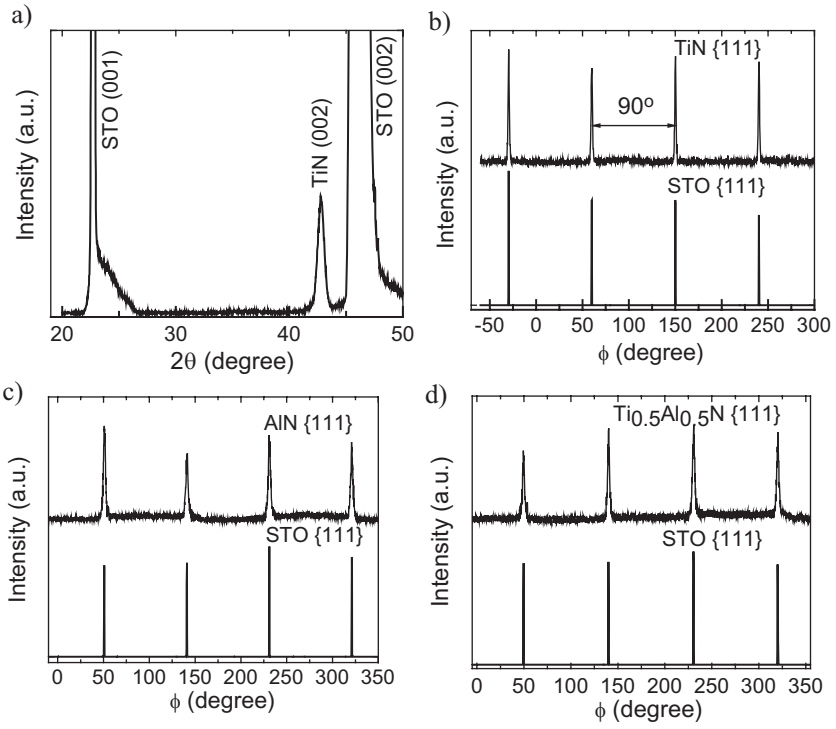

Figure 1. XRD patterns: a) θ–2θ scan for TiN/STO, b) ϕ-scans from (111) reflections of TiN and STO, c) ϕ-scans from (111) reflections of AlN and STO, and d) ϕ-scans from (111) reflections of $Ti_{0.5}Al_{0.5}N$ and STO.

Figure 1c and d show the XRD ϕ-scans of AlN and $Ti_{0.5}Al_{0.5}N$ films on STO annealed at 1000 °C. XRD results show that no metal oxides exist in the nitride films. Only the (002) diffraction from the TiN film indicates that the film is preferentially oriented along the *c*-axis, perpendicular to the substrate surface. The in-plane orientation between the films and the substrates was determined by XRD ϕ-scans from (111) STO and (111) TiN, AlN, and ($Ti_{0.5}Al_{0.5}N$) films. Four peaks with separations of 90 ° in the ϕ-scans indicate the epitaxial nature of the films. The epitaxial relationships can be described as $(001)_{(Ti,Al)N}||(001)_{STO}$ and $[111]_{(Ti,Al)N}||[111]_{STO}$. It is well known that the hexagonal AlN is a thermodynamically stable phase, while cubic AlN is metastable. Indeed, epitaxial hexagonal AlN films have been reported on sapphire substrates grown by MOCVD, pulsed-laser deposition, and lateral epitaxial overgrowth.[3,20,21] Very recently, cubic AlN films were grown epitaxially on STO substrates by pulsed-laser deposition.[23] We have demonstrated that the metastable phase can be stabilized and fabricated by taking advantage of the heteroepitaxy, where the crystallographic order of the films can be controlled by the substrates.[43]

In addition to these binary nitrides, the solid-solution cubic $Ti_{1-x}Al_xN$ films on STO can also be formed by this simple approach. Figure 2 shows the Rutherford backscattering spectrometry (RBS) spectrum (black curve) of a nominal $Ti_{0.5}Al_{0.5}N$ film on quartz, together with a fit (red). We choose quartz as substrate for the RBS measurement since the Ti or Al from STO or $LaAlO_3$ substrates render it very difficult to accurately determine the Ti/Al ratio in the film. As can be seen in Figure 2, major elements Ti, Al, N, and O were observed in the film, together with Si and O from the substrate. The RBS analysis results in a Ti/Al ratio of 0.56:0.44 (the statistical errors for Ti and Al are 2.3 and 4.5%, respectively), in good agreement with the nominal predetermined 0.5:0.5 from the solutions. Notably, oxygen was also detected in the film from RBS analysis. With the overlap of the N signal from the film with the O signal from the substrate, and the much larger statistical errors obtained for O (~16%) and N (~24%) from the RBS measurement, it is very difficult for us to accurately determine the amounts of O and N in the films. Carbon contamination in the nitrides is also a concern, since the precursors used in the film growth contain polymers.[37] We detected carbon from the $Ti_{0.5}Al_{0.5}N$ film in the X-ray photoelectron spectroscopy (XPS) analysis, however, it is difficult to obtain a quantitative evaluation of carbon content in the film from such measurements.

The surface morphology of the films was investigated by both scanning electron microscopy (SEM) and atomic force microscopy (AFM). Figure 3 shows an SEM image of a $Ti_{0.5}Al_{0.5}N$ film annealed at 1000 °C and AFM images of the $Ti_{0.5}Al_{0.5}N$ films on STO annealed at 900 °C and 1000 °C, respectively. As can be seen from these images, the films are dense, with no detectable microcracks. The films have average grain sizes (surface) of around 13 nm, for the $Ti_{0.5}Al_{0.5}N$ film annealed at 900 °C, and 18 nm, for the film annealed at 1000 °C. The surface roughness is only about 0.3 nm (root mean square, rms) for the $Ti_{0.5}Al_{0.5}N$ films annealed at 900 °C or 1000 °C.

Figure 4a shows a cross-section bright-field transmission electron microscopy (TEM) image of a $Ti_{0.5}Al_{0.5}N$ film on STO, and Figure 4b and c show the cross-section high-resolution TEM (HRTEM) images of the interfaces between a $Ti_{0.5}Al_{0.5}N$ film and STO and a AlN film and STO, respectively. The inset in Figure 4a shows the corresponding selected-area electron-diffraction

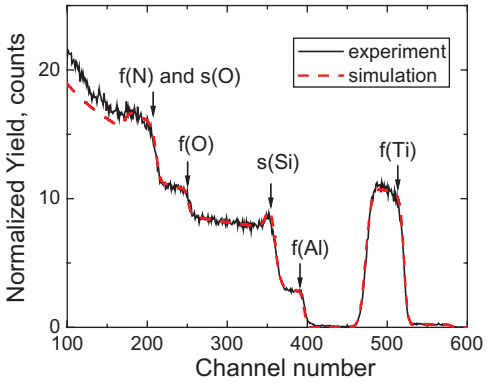

Figure 2. RBS spectrum (black) and fit (red) of a nominal $Ti_{0.5}Al_{0.5}N$ film on quartz glass. Note: f = film, s = quartz substrate. Measurements were performed with 2 MeH He^+ beam, and the sample was tilted 75° to avoid overlapping of Al and Si signals.

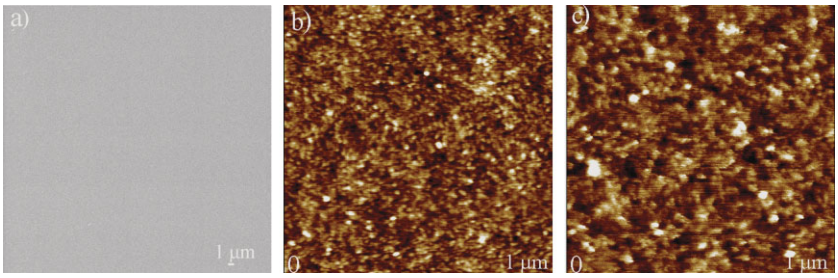

Figure 3. SEM image of $Ti_{0.5}Al_{0.5}N$ film annealed at 1000 °C a) and AFM images of $Ti_{0.5}Al_{0.5}N$ film annealed at 900 °C b) and 1000 °C c), respectively.

(SAED) pattern from the interface between the $Ti_{0.5}Al_{0.5}N$ film and the STO substrate. The SAED pattern shows a typical cube-on-cube epitaxial relationship between the film and the substrate, evidenced by the distinguished diffraction dots, consistent with the XRD results. From the low-magnification image (Fig. 4a), it is obvious that the film has good surface coverage, and a thickness of about 90 nm. This film contains some subgrain structures based on the existence of contrast differences. These differences are thought to be due to the small tilting between the subgrain structures. This typical sample was annealed at 1000 °C for 1 h. It is noted that, for the same annealing conditions, TiN films have better surface coverage and better crystallinity than AlN. Thus, a higher annealing temperature is needed for AlN than that for TiN. For instance, XRD ϕ-scans and TEM analysis show that TiN is epitaxial when the film was annealed at 900 °C for 1 h. However, the crystallinity of $Ti_{0.5}Al_{0.5}N$ and AlN are low for these conditions. A relatively higher annealing temperature (~1000 °C) or a longer annealing time (3 h at 900 °C) is needed for the formation of epitaxial AlN and $Ti_{0.5}Al_{0.5}N$ films.

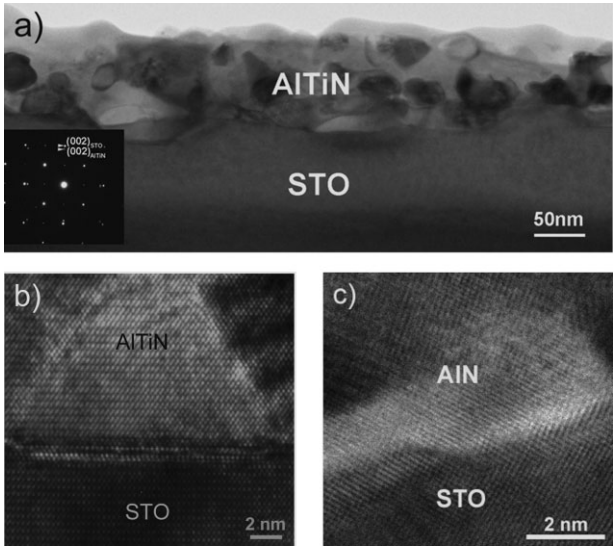

Figure 4. a) A bright-field TEM image of a cubic $Ti_{0.5}Al_{0.5}N$ film on STO. The insert shows the SAED pattern taken from the interface between the film and the substrate. Cross-section HRTEM images taken from the interface of b) $Ti_{0.5}Al_{0.5}N$ and STO and c) AlN and STO.

Figure 5 shows the optical transmission characteristics of $Ti_{1-x}Al_xN$ ($x = 0$–0.5 and 1) films. As expected, AlN films are highly transparent, with optical transmittance greater than 75% at wavelengths in the range of 300–1100 nm. The transmittance decreases with increasing Ti content in $Ti_{1-x}Al_xN$ films. It is interesting to note that the resistivities of these nitrides are a strong function of Ti/Al ratio.[44] Figure 6 shows the temperature-dependent resistivities of TiN films annealed at 900 °C and $Ti_{1-x}Al_xN$ ($x = 0.1$ and 0.2) films annealed at 1000 °C. As can be seen in the figure, TiN films are highly conductive, with a resistivity of around $1.9 \times 10^{-5}\ \Omega \cdot cm$ at room temperature. Similarly to the TiN films prepared by other deposition techniques, our TiN films are metallic. In other words, the resistivity of our TiN decreases with decreasing temperatures. On the other hand, $Ti_{0.9}Al_{0.1}N$ films are metallic between 300 and 100 K, and adopt a semiconductor behavior from 100 to 5 K. With increasing Al contents in $Ti_{1-x}Al_xN$ ($x = 0.2$–0.5) films, a semiconductor behavior is shown from 300 to 5 K. Furthermore, the room-temperature resistivity of the films increases exponentially with the increase in Al content in $Ti_{1-x}Al_xN$, as shown in Figure 7. In comparison, the resistivity of a AlN film is in the range of $10^{11} - 10^{14}\ \Omega \cdot cm$.[29] In addition, high annealing temperatures lead to lower resistivities for $Ti_{1-x}Al_xN$ ($x = 0.1$–0.5) films. For example, the resistivity of a $Ti_{0.56}Al_{0.44}N$ film is reduced from 2×10^{-1} to $8.5 \times 10^{-2}\ \Omega \cdot cm$ when the annealing temperature is increased from 900 °C to 1000 °C.

In summary, we report the growth of smooth epitaxial cubic TiN, metastable cubic AlN, and solid-solution cubic $Ti_{1-x}Al_xN$ thin films using PAD, a chemical solution approach. The TiN films are highly conductive, and the AlN films are highly transparent. The room-temperature electrical resistivity of the $Ti_{1-x}Al_xN$ films increases exponentially with increasing Al contents, while the optical transmittance decreases with increasing Ti content. This solution-deposition technique provides an alternative for epitaxial growth of nitride films. Importantly, the formation of complex metal nitride systems using PAD is simple,

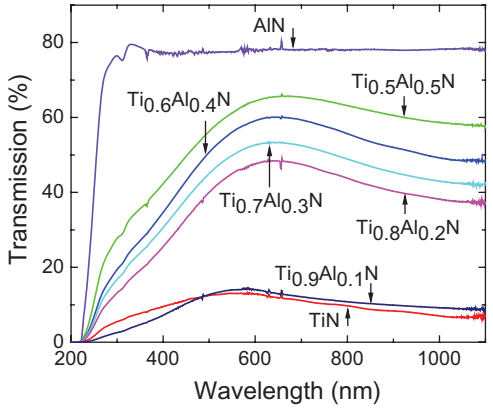

Figure 5. Optical transmittance spectra for nominal $Ti_{1-x}Al_xN$ ($x = 0$–0.5, 1) films on double-side polished LAO (TiN film was annealed at 900 °C, and other films were annealed at 1000 °C). Films thickness is around 60 nm.

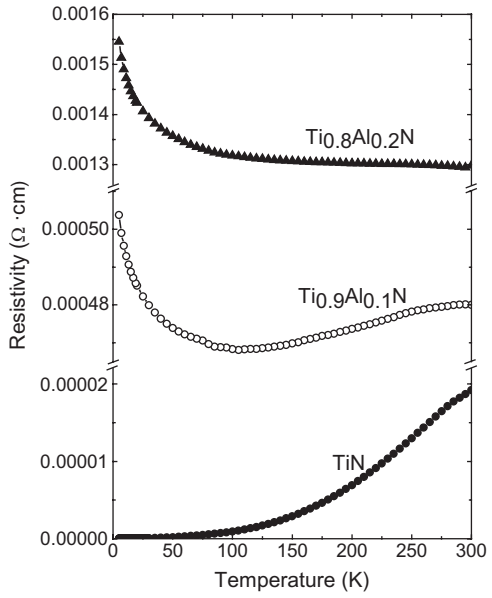

Figure 6. Temperature-dependent resistivities of a TiN film annealed at 900 °C and $Ti_{1-x}Al_xN$ ($x = 0.1$–0.2) films on STO annealed at 1000 °C.

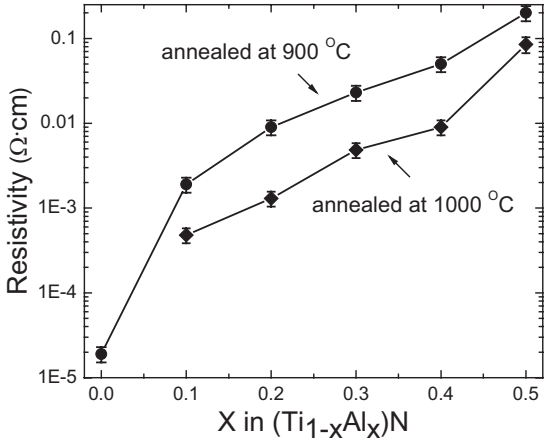

Figure 7. Room-temperature resistivity of nominal $Ti_{1-x}Al_xN$ ($x = 0$–0.5) films annealed at 900 °C and 1000 °C.

requiring only the control of the stoichiometry of metal ions in the polymer precursors.

Experimental

Sample Preparation: The precursors for the growth of TiN, AlN, and $Ti_{1-x}Al_xN$ films were prepared using aqueous solutions of Ti and Al bound to polymers PEI and/or EDTA. Both PEI and EDTA were purchased from BASF Corporation of Clifton, NJ, and were used without further purification. Ultrafiltration was carried out by repeated Amicon filtration, which retains the high molecular weight polymer with bound metal atoms, while allows any low molecular weight ($<10\,000$ g mol^{-1}) species to pass through. Metal concentration analysis was conducted using a Varian Liberty 220 inductively coupled plasma–atomic emission spectrometer (ICP–AES), following the standard SW846 EPA (Environmental Protection Agency) Method 6010 procedure.

To prepare Ti–polymer solutions, the titanium solution (2.5 g titanium tetrachloride was added slowly to a mixture of 2.5 g of 30% peroxide in 30 mL of water) was added to a solution containing 1 g PEI, 1 g EDTA, and 30 mL water, until precipitation occurred (the pH was maintained at 7.5). For the Al–polymer solution, aluminum nitrate was mixed with a fluorinated PEI polymer (PEIF, prepared by slowly adding 5 mL 48% hydrofluoric acid to 10 g PEI in 40 mL water, while maintaining the pH at 7). Specifically, 2 g aluminum nitrate hydrate was added to 3 g PEIF in 40 mL water. The final concentrations were 408 mM for Ti and 201 mM for Al. The individual Ti or Al solution was spin-coated onto (001) $SrTiO_3$ (STO) or $LaAlO_3$ (LAO) substrates at 2000 rpm for 30 s. To prepare $Ti_{1-x}Al_xN$ films, the precursor solutions with desired stoichiometric molar ratios for $x = 0.1$–0.5 from Ti and Al solutions were spin-coated onto STO or LAO. The films were heated in forming gas (4% H_2 and 96% N_2) at 510 °C for 2 h, and then annealed in ammonia gas at 900 °C for 1 h for TiN films, 1000 °C for 1 h for AlN films, and 900 or 1000 °C for 1 h for $Ti_{1-x}Al_xN$ films. It should be noted that $Ti_{0.5}Al_{0.5}N$ films were also coated on quartz slides, and annealed at 1000 °C for 1 h for composition analysis. Films with a thickness in the range of 40–50 nm were obtained from one spin-coated layer. Thicker films could be deposited by spin-coating multiple layers.

Sample Characterization: XRD was used to characterize the crystallographic orientation of the films. The surface morphology and surface roughness of the films were analyzed by SEM and AFM. The microstructure of the films was analyzed using TEM. The composition of the films was determined using RBS. The optical properties of the films were examined using UV–vis transmittance at room temperature. The electrical resistivity (ρ) of the films was measured based on a standard four-probe technique using a physical-property measurement system (PPMS) from Quantum Design.

Acknowledgements

We gratefully acknowledge the support of the US Department of Energy (DOE) through the LANL/LDRD Program, DOE EE-RE Solid State Lighting Program, and NSF/DMR Ceramic Program (NSF 0709831).

Received: July 10, 2008
Published online: October 30, 2008

[1] S. Strite, H. Morkoc, *J. Vac. Sci. Technol. B* **1992**, *10*, 1237.
[2] S. B. S. Heil, E. Langereis, F. Roozeboom, M. C. M. van de Sanden, W. M. M. Kessels, *J. Electrochem. Soc.* **2006**, *153*, G956.
[3] Q. S. Paduano, D. W. Weyburne, J. Jasinski, Z. Liliental-Weber, *J. Cryst. Growth* **2004**, *261*, 259.
[4] P. W. Shum, K. Y. Li, Z. F. Zhou, Y. G. Shen, *Surf. Coat. Technol.* **2004**, *185*, 245.
[5] J. Musil, H. Hrubý, *Thin Solid Films* **2000**, *365*, 104.
[6] T. T. Leung, C. W. Ong, *Diamond Relat. Mater.* **2004**, *13*, 1603.
[7] Y. Tanaka, T. M. Gur, M. Kelly, S. B. Hagstrom, T. Ikeda, *Thin Solid Films* **1993**, *228*, 238.
[8] U. Wahlström, L. Hultman, J.-E. Sundgren, F. Adibi, I. Petrov, J. E. Greene, *Thin Solid Films* **1993**, *235*, 62.
[9] R. Wuhrer, W. Y. Yeung, M. R. Phillips, G. McCredie, *Thin Solid Films* **1996**, *290*, 339.
[10] M. Zhou, Y. Makino, M. Nose, K. Nogi, *Thin Solid Films* **1999**, *339*, 203.
[11] J. Y. Rauch, C. Rousselot, N. Martin, *Surf. Coat. Technol.* **2002**, *157*, 138.
[12] Y. Matsui, M. Hiratani, Y. Nakamura, I. Asano, F. Yano, *J. Vac. Sci. Technol. A* **2002**, *20*, 605.
[13] C. G. Zhang, L. F. Bian, W. D. Chen, C. C. Hsu, *J. Cryst. Growth* **2007**, *299*, 268.

[14] G. Abadias, Y. Y. Tse, *Surf. Coat. Technol.* **2004**, *180–181*, 33.
[15] Y. Sesuhara, T. Suzuki, Y. Makino, S. Miyake, T. Sakata, H. Mori, *Surf. Coat. Technol.* **1997**, *97*, 254.
[16] Y. H. Cheng, B. K. Tay, S. K. Tay, S. P. Lau, X. Shi, *J. Vac. Sci. Technol. A* **2001**, *19*, 736.
[17] P. K. Kuo, G. W. Auner, Z. L. Wu, *Thin Solid Films* **1994**, *253*, 223.
[18] A. Sidorenko, H. Peisert, H. Neumann, T. Chassé, *Appl. Surf. Sci.* **2006**, *252*, 7671.
[19] J. W. Gerlach, A. Hofmann, T. Höche, F. Frost, B. Rauschenbach, G. Benndorf, *Appl. Phys. Lett.* **2006**, *88*, 011902.
[20] S. Six, J. W. Gerlach, B. Rauschenbach, *Thin Solid Films* **2000**, *370*, 1.
[21] Z. Chen, R. S. Q. Fareed, M. Gaevski, V. Adivarahan, J. W. Yang, A. Khan, J. Mei, F. A. Ponce, *Appl. Phys. Lett.* **2006**, *89*, 081905.
[22] S. Bakalova, A. Szekeres, S. Grigorescu, E. Axente, G. Socol, I. N. Mihailescu, *Appl. Phys. A* **2006**, *85*, 99.
[23] J. Zhu, D. Zhao, W. B. Luo, Y. Zhang, Y. R. Li, *J. Crys. Growth* **2008**, *310*, 731.
[24] D. Cai, L. L. Zheng, H. Zhang, V. L. Tassev, D. F. Bliss, *J. Cryst. Growth* **2005**, *276*, 182.
[25] K. Kusakabe, S. Ando, K. Ohkawa, *J. Cryst. Growth* **2007**, *298*, 293.
[26] S.-H. Lee, B.-J. Kim, H.-H. Kim, J.-J. Lee, *J. Appl. Phys.* **1996**, *80*, 1469.
[27] J. Shieh, M. H. Hon, *Thin Solid Films* **2001**, *391*, 101.
[28] S. Shimada, Y. Takada, J. Tsujino, *J. Eur. Ceram. Soc.* **2005**, *25*, 1765.
[29] S. Ikeda, S. Gilles, B. Chenevier, *Thin Solid Films* **1998**, *315*, 257.
[30] J. T. Scheper, K. W. Mesthrige, J. W. Proscia, G.-Y. Liu, C. H. Winter, *Chem. Mater.* **1999**, *11*, 3490.
[31] Y.-H. Shin, Y. Shimogaki, *Jpn. J. Appl. Phys.* **2004**, *43*, 8253.
[32] J. Jasinski, *Phys. Status Solidi C* **2005**, *3*, 994.
[33] F. F. Lange, *Science* **1996**, *273*, 903.
[34] M. Puchinger, T. Wagner, D. Rodewald, J. Bill, F. Aldinger, F. F. Lange, *J. Cryst. Growth* **2000**, *208*, 153.
[35] M. Puchinger, D. J. Kisailus, F. F. Lange, T. Wagner, *J. Cryst. Growth* **2002**, *245*, 219.
[36] H. Parala, A. Devi, A. Wohlfart, M. Winter, R. A. Fischer, *Adv. Funct. Mater.* **2001**, *11*, 224.
[37] D. Kisailus, J. H. Choi, F. F. Lange, *J. Mater. Res.* **2002**, *17*, 2540.
[38] T. P. Niesen, M. Puchinger, P. Gerstel, D. Rodewald, J. Wolff, T. Wagner, J. Bill, F. Aldinger, *Mater. Chem. Phys.* **2002**, *73*, 301.
[39] K. Sardar, A. R. Raju, G. N. Subbanna, *Solid State Commun.* **2003**, *125*, 355.
[40] A. L. Hector, *Chem. Soc. Rev.* **2007**, *36*, 1745.
[41] Q. X. Jia, T. M. McCleskey, A. K. Burrell, Y. Lin, G. E. Collis, H. Wang, A. D. Q. Li, S. R. Foltyn, *Nat. Mater.* **2004**, *3*, 529.
[42] A. K. Burrell, T. M. McCleskey, Q. X. Jia, *Chem. Commun.* **2008**, 1271.
[43] A. K. Burrell, T. M. McCleskey, P. Shukla, H. Wang, T. Durakiewicz, D. P. Moore, C. G. Olson, J. J. Joyce, Q. X. Jia, *Adv. Mater.* **2007**, *19*, 3559.
[44] I.-L. Tangen, Y. Yu, T. Grande, R. Høier, M.-A. Einarsrud, *J. Eur. Ceram. Soc.* **2004**, *24*, 2169.